

# Discovery of novel urokinase plasminogen activator (uPA) inhibitors using ligand-based modeling and virtual screening followed by in vitro analysis

Mahmoud A. Al-Sha'er · Mohammad A. Khanfar · Mutasem O. Taha

Received: 18 August 2013 / Accepted: 28 October 2013  
© Springer-Verlag Berlin Heidelberg 2013

**Abstract** Urokinase plasminogen activator (uPA)—a serine protease—is thought to play a central role in tumor metastasis and angiogenesis and, therefore, inhibition of this enzyme could be beneficial in treating cancer. Toward this end, we explored the pharmacophoric space of 202 uPA inhibitors using seven diverse sets of inhibitors to identify high-quality pharmacophores. Subsequently, we employed genetic algorithm-based quantitative structure-activity relationship (QSAR) analysis as a competition arena to select the best possible combination of pharmacophoric models and physicochemical descriptors that can explain bioactivity variation within the training inhibitors ( $r^2_{162}=0.74$ , F-statistic=64.30,  $r^2_{\text{LOO}}=0.71$ ,  $r^2_{\text{PRESS}}$  against 40 test inhibitors=0.79). Three orthogonal pharmacophores emerged in the QSAR equation suggesting the existence of at least three binding modes accessible to ligands within the uPA binding pocket. This conclusion was supported by receiver operating characteristic (ROC) curve analyses of the QSAR-selected pharmacophores. Moreover, the three pharmacophores were comparable with binding interactions seen in crystallographic structures of bound ligands within the uPA binding pocket. We employed the resulting pharmacophoric models and associated QSAR equation to screen the national cancer institute (NCI) list of compounds. The captured hits were tested

in vitro. Overall, our modeling workflow identified new low micromolar anti-uPA hits.

**Keywords** Urokinase plasminogen activator · Ligand based analysis · Serine peptidase · Anticancer · Anti-inflammatory

## Introduction

Urokinase-type plasminogen activator (uPA)

Urokinase-type plasminogen activator (uPA) is a serine protease that has been implicated as a key mediator of cellular invasion and tissue remodeling [1]. An inhibitor of uPA may have a therapeutic role in disease situations where uPA-driven degradation of extracellular matrix, or uPA-dependent cell migration is thought to be important including tumor growth, metastasis, angiogenesis and chronic wounds [2–7].

Evidence has also been obtained to suggest that uPA, or plasmin produced by its action, may play a role in preventing healing of chronic wounds [3, 7]. Consequently, a selective inhibitor for uPA could have therapeutic value in cancer and wound healing [1, 7].

The main focus of recent efforts towards the development of new uPA inhibitors concentrate on structure-based ligand design [8–10] and high throughput screening [11, 12]. To date, several uPA X-ray complexes are documented in the Protein Data Bank (e.g., PDB codes: 1OWD, 1OWE, 1SQO, 1SQT, 1SQA, 1CFL, 1EJN, 1OWH, 1OWK, 1OWJ, 1U6Q, 1YWH, 2OW8) with good resolution. However, although crystallographic structures are generally considered the most reliable structural information for drug design purposes, they are limited by inadequate resolution [13] and crystallization-related artifacts of the ligand–protein complex [14–16]. Moreover, crystallographic structures generally ignore structural

**Electronic supplementary material** The online version of this article (doi:10.1007/s00894-013-2056-9) contains supplementary material, which is available to authorized users.

M. A. Al-Sha'er  
Faculty of Pharmacy, Zarqa University, Zarqa 13132, Jordan  
e-mail: a.mahmoud@zu.edu.jo

M. A. Khanfar · M. O. Taha (✉)  
Department of Pharmaceutical Sciences, Faculty of Pharmacy,  
University of Jordan, Amman, Jordan  
e-mail: mutasem@ju.edu.jo

68 heterogeneity related to protein anisotropic motion and dis- 115  
69 crete conformational substrates [17]. 116

70 The continued interest in designing new uPA inhibitors and 117  
71 the lack of adequate ligand-based computer-aided drug dis- 118  
72 covery efforts, which can overcome the drawbacks of 119  
73 structure-based design, combined with the significant induced 120  
74 fit flexibility observed for uPA [18], prompted us to explore 121  
75 the possibility of developing ligand-based three-dimensional 122  
76 (3D) pharmacophore(s) integrated within a self-consistent 123  
77 quantitative structure-activity relationship (QSAR) model. 124  
78 This approach avoids the pitfalls of structure-based tech- 125  
79 niques; furthermore, the pharmacophore model(s) can be used 126  
80 as 3D search queries to discover new uPA inhibitory scaffolds. 127  
81 We previously reported the use of this innovative approach  
82 towards the discovery of new inhibitory leads against glyco-  
83 gen synthase kinase-3 $\beta$ , [19] bacterial MurF [20], protein  
84 tyrosine phosphatase [21], DPP IV [22], hormone sensitive  
85 lipase [23],  $\beta$ -secretase [24], influenza neuraminidase [25],  
86 migration inhibitory factor [26], cyclin dependent kinase in-  
87 hibitors (CDK1)[27], and heat shock protein 90 (Hsp90) [28].

## 88 Methods

### 89 Molecular modeling

90 Pharmacophore and QSAR modeling studies were performed 129  
91 using the CATALYST (HYPOGEN module) [33] and 130  
92 CERIUS2 software suites implemented in Discovery Studio 131  
93 2.5.5 from Accelrys Inc. (San Diego, CA,, [http://www.](http://www.accelrys.com) 132  
94 [accelrys.com](http://www.accelrys.com)). Structure drawing was performed employing 133  
95 ChemDraw Ultra 7.0 (Cambridge Soft Corp. ([http://www.](http://www.cambridgesoft.com) 134  
96 [cambridgesoft.com](http://www.cambridgesoft.com)), Cambridge, MA). 135

### 97 Data set and conformational analysis

98 The structures of 202 uPA inhibitors (**1–202**, Fig. 1, Table A 129  
99 in the electronic supplementary material) were collected from 130  
100 recently published literature [29–36]. Although the in vitro 131  
101 bioactivities of the collected inhibitors were gathered from 132  
102 separate articles, the fact that the bioactivities were expressed 133  
103 as affinity values ( $K_i$ ) should minimize any discrepancies 134  
104 resulting from variations in bioassay procedure [26]. The 135  
105 logarithm transformation of  $K_i$  ( $\mu\text{M}$ ) values were used in 136  
106 QSAR and pharmacophore modeling, thus linearly correlating 137  
107 the bioactivities with binding free energy change. 138

108 The two-dimensional (2D) chemical structures of the in- 129  
109 hibitors were sketched using ChemDraw Ultra and saved in 130  
110 MDL-molfile format. Subsequently, they were imported into 131  
111 CATALYST, converted into corresponding standard 3D struc- 132  
112 tures and energy minimized to the closest local minimum 133  
113 using the molecular mechanics CHARMM force field 134  
114 implemented in CATALYST. The resulting 3D structures 135

116 were utilized as starting conformers for CATALYST 117  
118 conformational analysis. 119

120 The conformational space of collected each inhibitor (**1–** 121  
122 **202**, Fig. 1, Table A under electronic supplementary material) 123  
124 was explored adopting the “best conformer generation” option 125  
126 within CATALYST [37] based on the generalized CHARMM 127  
128 force field implemented in the program. Default parameters  
129 were employed in the conformation generation procedure of  
130 training compounds and screened libraries, i.e., a conforma-  
131 tional ensemble was generated with an energy threshold of  
132 20 kcal/mol<sup>-1</sup> from the local minimized structure at which has  
133 the lowest energy level and a maximum limit of 250 con-  
134 formers per molecule [37, 38]. 135

### 128 Generation and assessment of binding hypotheses

129 All 202 molecules with their associated conformational 129  
130 models were grouped into a spreadsheet. The biological data 130  
131 of the inhibitors were reported with an “Uncertainty” value of 131  
132 three, which means that the actual bioactivity of a particular 132  
133 inhibitor is assumed to be situated somewhere in an interval 133  
134 ranging from one-third to three-times the reported bioactivity 134  
135 value of that inhibitor [39, 40]. Subsequently, seven structur- 135  
136 ally diverse training subsets were selected: subsets **I**, **II**, **III**, 136  
137 **IV**, **V**, **VI** and **VII** shown in Table B in the electronic supple- 137  
138 mentary material. The selected training sets were utilized to 138  
139 conduct 48 modeling runs to explore the pharmacophoric 139  
140 space of uPA inhibitors. Table C of the supplementary materi- 140  
141 al shows the training subsets and different parameters im- 141  
142 plemented for each pharmacophore exploration run. The ex- 142  
143 ploration process included altering number and type of possi- 143  
144 ble binding features (hydrogen bond acceptors, hydrogen 144  
145 bond donors, aromatic rings, ionizable groups and hydropho- 145  
146 bic features), feature spacing parameter (100 and 300 pm) and 146  
147 the maximum number of allowed features in the resulting 147  
148 pharmacophore hypotheses. 148

149 Pharmacophore modeling employing CATALYST pro- 149  
150 ceeds through three consecutive steps: the constructive phase, 150  
151 subtractive phase and optimization phase (see CATALYST 151  
152 Modeling Algorithm under section **SM-1** in [Supplementary](#) 152  
153 [Materials](#)) [37–43]. In the optimization phase, CATALYST 153  
154 attempts to minimize a cost function for each hypotheses 154  
155 consisting of three terms: Weight cost, Error cost and Config- 155  
156 uration cost (see CATALYST Cost Analysis in Assessment of 156  
157 Generated Binding Hypotheses under section **SM-2** in [Sup-](#) 157  
158 [plementary Materials](#)). 158

159 CATALYST-HYPOGEN cross-validates the resulting opti- 159  
160 mal pharmacophores using the Cat-Scramble module imple- 160  
161 mented in CATALYST. This validation procedure is based on 161  
162 Fischer’s randomization test [44]. In this validation test; we 162  
163 selected a 95 % confidence level, which instructs CATALYST 163  
164 to generate 19 random spreadsheets by the Cat-Scramble 164  
165 command. Subsequently, CATALYST-HYPOGEN is 165

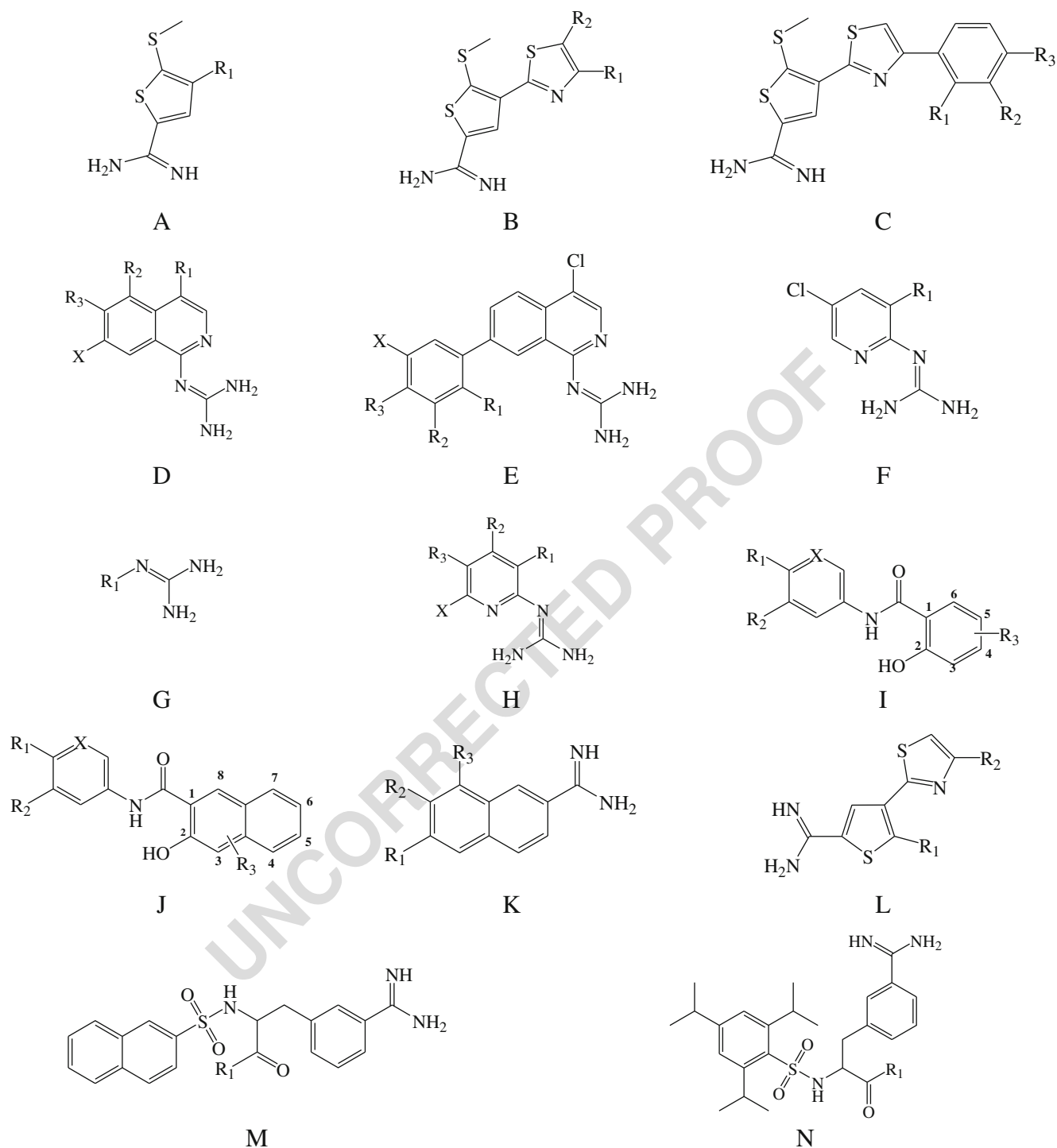


**Fig. 1** Chemical scaffolds for urokinase plasminogen activator (uPA)

166 challenged to use these random spreadsheets to generate  
 167 hypotheses using exactly the same features and param-  
 168 eters used in generating the initial unscrambled hypoth-  
 169 eses. Success in generating pharmacophores of compa-  
 170 rable cost criteria to those produced by the original  
 171 unscrambled data reduces the confidence in the training

172 compounds and the unscrambled original pharmacophore 172  
 173 models [37, 44, 45]. Based on Fischer randomization 173  
 174 criteria; all 480 pharmacophores exceeded the 95 % 174  
 175 significance threshold for subsequent processing. 175  
 176 Table D under [Supplementary Materials](#) shows different 176  
 177 cost criteria and significance levels of representative 177

178	pharmacophoric hypotheses (see pharmacophore cluster-	227
179	ing under <b>QSAR modeling</b> section).	228
180	<i>QSAR modeling</i>	229
181	The resulting pharmacophore models (480) were clustered into	230
182	45 groups utilizing the hierarchical average linkage method	231
183	available in CATALYST. Subsequently, the highest-ranking	232
184	representatives, as judged based on their significance F-values	233
185	(calculated from correlating their fit values against the whole	234
186	list of collected compounds with the corresponding molecular	235
187	bioactivities) were selected to represent their corresponding	236
188	clusters in subsequent QSAR modeling. Table D under Sup-	
189	plementary Materials shows information about representative	
190	pharmacophores including their pharmacophoric features, suc-	
191	cess criteria and differences from corresponding null hypothe-	
192	ses. The Table also shows the corresponding Cat. Scramble	
193	confidence levels for each representative pharmacophore.	
194	QSAR modeling commenced by selecting a subset of 162	
195	compounds from the total list of inhibitors (1–202, Fig. 1,	
196	Table A under Supplementary Materials) as a training set for	
197	QSAR modeling; the remaining 40 molecules (ca. 20 % of the	
198	dataset) were employed as an external test subset for validat-	
199	ing the QSAR models. The test molecules were selected as	
200	follows: all 202 inhibitors were ranked according to their $K_i$	
201	values, and then every fifth compound was selected for the test	
202	set starting from the high-potency end. The selected test	
203	molecules should represent similar range of biological activ-	
204	ities to that of the training set. The selected test inhibitors are	
205	marked with asterisks in Table A under Supplementary	
206	Materials.	
207	The logarithm of measured $K_i$ ( $\mu\text{M}$ ) values was used in	
208	QSAR, thus correlating the data linear to the free energy	
209	change. Subsequently, we implemented genetic algorithm	
210	and multiple linear regression analyses to select optimal com-	
211	bination of pharmacophoric models and other physicochemi-	
212	cal descriptors capable of self-consistent and predictive QSAR	
213	model. Section SM-3 under <b>Supplementary Materials</b> de-	
214	scribes extensively the experimental details of QSAR model-	
215	ing procedure [37, 46].	
216	<i>Addition of exclusion volumes</i>	
217	To account for the steric constrains of the binding pocket, we	
218	decided to complement our QSAR-selected pharmacophore	
219	models (i.e., Hypo34/2, Hypo37/3 and Hypo38/10) with ex-	
220	clusion volumes employing Hip-Hop-Refine module of CAT-	
221	ALYST. Hip-Hop-Refine uses inactive training compounds to	
222	construct excluded volumes that resemble the steric constrains	
223	of the binding pocket. It identifies spaces occupied by the	
224	conformations of inactive compounds and free from active	
225	ones. These regions are then filled with excluded volumes	
226	[21–23, 37]. Subset VIII (in Table E under Supplementary	
	Material) was used to construct exclusion spheres around	227
	Hypo34/2, Hypo37/3 and Hypo38/10. Section SM-4 under	228
	<b>Supplementary Materials</b> describes in details the Hip-Hop-	229
	Refine algorithm and settings implemented herein to decorate	230
	Hypo34/2, Hypo37/3 and Hypo38/10 with exclusion spheres.	231
	The resulting sterically refined pharmacophores, as well as	232
	their unrefined versions, were validated by receiver operating	233
	characteristic curve analysis (ROC). [47–50], Theoretical and	234
	experimental details of this procedure are as shown in section	235
	SM-5 under <b>Supplementary Material</b> .	236
	<i>In silico screening for new uPA inhibitors</i>	237
	The sterically refined versions of Hypo34/2, Hypo37/3 and	238
	Hypo38/10 were employed as 3D search queries to screen the	239
	3D flexible molecular database of the National Cancer Insti-	240
	tute (NCI). The screening was done employing “Best Flexible	241
	Database Search” option implemented within CATALYST.	242
	Captured hits were filtered according to Lipinski’s [51] and	243
	Veber’s [49] rules. Remaining hits were fitted against	244
	Hypo34/2, Hypo37/3 and Hypo38/10 using the “best fit”	245
	option within CATALYST via implementing equation (D) in	246
	section SM-2 under <b>Supplementary Materials</b> . The fit values	247
	together with the relevant molecular descriptors of each hit	248
	were substituted in the optimal QSAR equation. The highest	249
	ranking molecules based on QSAR predictions were acquired	250
	and tested in vitro.	251
	<i>In vitro experimental studies</i>	252
	<i>Materials</i>	253
	All chemicals used in these experiments were of reagent grade	254
	and obtained from commercial suppliers. NCI samples were	255
	kindly provided by the National Cancer Institute ( <a href="http://www.cancer.gov/">http://www.cancer.gov/</a> ).	256
	<i>Quantification of the anti-uPA bioactivities of different hits</i>	258
	Bioassays were performed using the CHEMICON uPA kit for	259
	screening of uPA inhibitors [52]. The assay kit utilizes a	260
	chromogenic substrate, which is cleaved by active uPA en-	261
	zyme. Addition of this substrate to a uPA-containing sample	262
	results in a colored product, detectable by its optical density at	263
	405 nm. The assay was conducted as described in the uPA	264
	assay kit. Assay mixture (200 $\mu\text{L}$ ) composed of uPA (2.5 U,	265
	2.5 $\mu\text{L}$ ), chromogenic substrate (L-pyroglutamyl-glycyl-L-argi-	266
	nine-p-nitroaniline hydrochloride, 20 $\mu\text{L}$ , 2.5 mg/ml),	267
	155 $\mu\text{L}$ deionized $\text{H}_2\text{O}$ (with or without inhibitor), and assay	268
	buffer (20 $\mu\text{L}$ , pH 7.4) was mixed and incubated at 37 °C for	269
	2 h. The absorbance of cleaved substrate was recorded at	270
	405 nm. Tested hit concentrations ranged from 1 $\mu\text{M}$ to	271
	50 $\mu\text{M}$ distributed log-linearly across the concentration range,	272



273 and at least two data points from each concentration were  
 274 collected. The  $IC_{50}$  value for each experiment was obtained  
 275 using nonlinear regression of the  $\log(\text{concentration})$  versus  
 276 percent inhibition values (GraphPad Prism 5.0, [http://www.  
 277 graphpad.com](http://www.graphpad.com)). The assay conditions were validated by  
 278 running positive (amiloride) and negative (deionized water)  
 279 controls [52].

## 280 Results and discussion

### 281 Exploration of uPA pharmacophoric space

282 A total of 202 compounds were used in this study (1–202, see  
 283 Fig. 1, Table A under supplementary material) [29–36]. We  
 284 decided to explore the pharmacophoric space of uPA inhibi-  
 285 tors through 48 HYPOGEN automatic runs and employing  
 286 seven selected training subsets: subsets I–VII in Table B  
 287 under supplementary material. The biological activity in the  
 288 training subsets spanned from 3.5 to 4.0 orders of magnitude.  
 289 The training compounds in these subsets were of maximal 3D  
 290 diversity and continuous bioactivity spread over more than 3.5  
 291 logarithmic cycles [42]. CATALYST-HYPOGEN was re-  
 292 stricted to explore pharmacophoric models incorporating from  
 293 zero to one PosIon, one NegIon feature, from zero to three  
 294 HBA, Hbic, and RingArom features, as shown in Table C  
 295 under supplementary material. The input features were reason-  
 296 ably selected based on visual evaluation of the training  
 297 compounds and comparison between the structures of potent,  
 298 moderate and inactive members. Furthermore, we instructed  
 299 the software to explore only four- and five-featured  
 300 pharmacophores, i.e., ignore models of lesser number of fea-  
 301 tures (as shown in Table C under supplementary material).  
 302 The reader is referred to section [Generation and Assessment  
 303 of Binding Hypotheses](#) in [Methods](#) and sections SM-1 and  
 304 SM-2 under [Supplementary Materials](#) for more details about  
 305 the CATALYST algorithm [38, 39, 42].

306 The resulting binding hypotheses from each automatic  
 307 pharmacophore modeling run were ranked automatically ac-  
 308 cording to their corresponding “total cost” value, which is de-  
 309 fined as the sum of error cost, weight cost and configuration cost  
 310 (see section [Generation and Assessment of Binding Hypotheses](#)  
 311 in [Methods](#) and section SM-2 under [Supplementary Materials](#))  
 312 [37–42]. Error cost provides the highest contribution to total cost  
 313 and is directly related to the capacity of the particular  
 314 pharmacophore as 3D-QSAR model, i.e., in correlating the  
 315 molecular structures to the corresponding biological responses  
 316 [37, 39–43]. HYPOGEN also calculates the cost of the null  
 317 hypothesis, which presumes that there is no relationship in the  
 318 data and that experimental activities are distributed normally  
 319 about their mean. Accordingly, the greater the difference from  
 320 the null hypothesis cost (i.e., residual cost, Table D under Sup-  
 321 plementary Materials) the more likely that the hypothesis does

not reflect a chance correlation. CATALYST implements an  
 additional validation technique based on Fisher’s randomization  
 test [45], namely, Cat.Scramble [37]. In this test, the biological  
 data and the corresponding structures are scrambled several  
 times and the software is challenged to generate pharmacophoric  
 models from the randomized data. The confidence in the parent  
 hypotheses (i.e., generated from unscrambled data) is lowered  
 proportional to the number of times the software succeeds in  
 generating binding hypotheses from scrambled data of apparent-  
 ly better cost criteria than the parent hypotheses (see  
 section [Generation and Assessment of Binding Hypotheses](#) in  
[Methods](#)) [37, 39–43].

Eventually, 480 pharmacophore models emerged from 48  
 automatic HYPOGEN runs, all of which exhibited Fisher  
 randomization confidence levels  $\geq 95\%$ . These successful  
 models were clustered and the best representatives (45  
 models, see section [Generation and Assessment of Binding  
 Hypotheses](#) under [Methods](#) and Table D under [Supplementary  
 Materials](#)) were used in subsequent QSAR modeling.

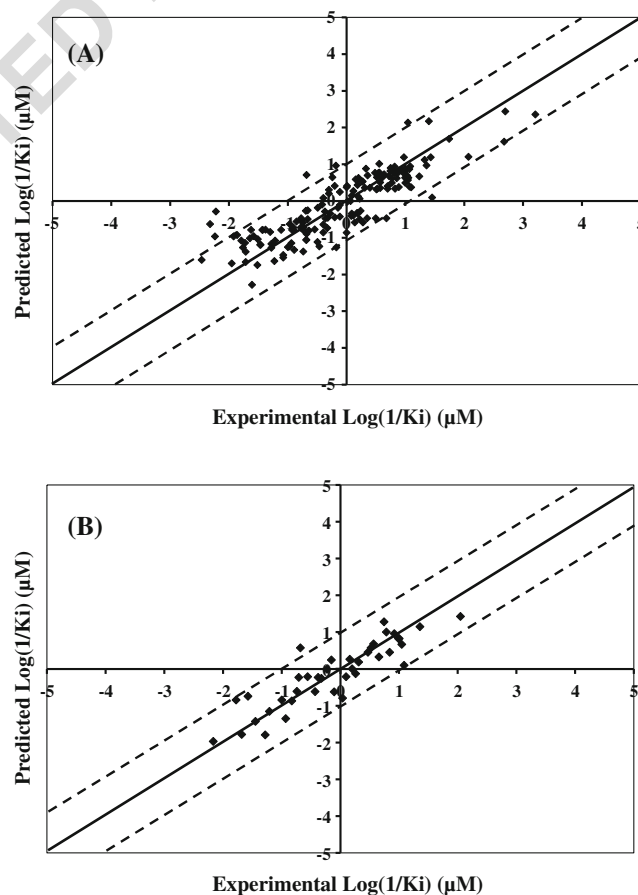


**Fig. 2** Experimental versus **a** fitted (162 training compounds,  $r^2_{\text{LOO}}=0.71$ ), and **b** predicted (40 test compounds,  $r^2_{\text{PRESS}}=0.79$ ) bioactivities calculated from the best quantitative structure-activity relationship (QSAR) model Eq. (1). *Solid lines* Regression lines for fitted and predicted bioactivities of training and test compounds, respectively; *dotted lines* 1.0 log point error margins

341 Interestingly, the representative models shared comparable  
342 features and acceptable statistical success criteria.

343 The emergence of several statistically comparable  
344 pharmacophore models suggests the ability of uPA ligands  
345 to assume multiple pharmacophoric binding modes within the  
346 binding pocket. Therefore, it is quite challenging to select any  
347 particular pharmacophore hypothesis as a sole representative  
348 of the binding process.

### 349 QSAR modeling

350 Despite the excellent value of pharmacophoric hypotheses in  
351 probing ligand–macromolecule recognition and as 3D search  
352 queries to search for new biologically interesting scaffolds,  
353 their predictive value as 3D-QSAR models is generally hamper-  
354 ed by steric shielding and bioactivity-enhancing or reducing  
355 auxiliary binding groups (e.g., the biological effects of  
356 electron-donating and withdrawing substitutions) [19–28].  
357 Moreover, our pharmacophore exploration of uPA inhibitors  
358 furnished hundreds of binding hypotheses of comparable suc-  
359 cess criteria, which makes it very hard to select any particular  
360 pharmacophore as sole representative of ligand binding within  
361 uPA. Accordingly, we were prompted to employ classical  
362 QSAR analysis to search for the best combination of  
363 pharmacophore(s) and other 2D descriptors capable of  
364 explaining bioactivity variation across the whole list of

365 collected inhibitors (1–202, Fig. 1, Table A). That is, we  
366 employed GFA-based QSAR as a competition arena to select  
367 the best pharmacophore(s), i.e., among the resulting population  
368 of binding models, and supplement it (them) with 2D descrip-  
369 tors to correct for the weaknesses of pharmacophore models  
370 (steric shielding and bioactivity-enhancing or reducing auxil-  
371 iary binding groups). We employed a genetic function approx-  
372 imation and multiple linear regression QSAR (GFA-MLR-  
373 QSAR) analysis to search for an optimal QSAR equation(s).

374 The fit values obtained by mapping representative hypoth-  
375 eses (45 models) against collected uPA inhibitors (1–202,  
376 Fig. 1, Table A) were enrolled, together with around 100 other  
377 physicochemical descriptors, as independent variables in  
378 GFA-MLR-QSAR analysis [19–28, 45, 54]. We randomly  
379 selected 40 molecules (marked with asterisks in  
380 Table A under Supplementary Materials) and employed  
381 them as external test molecules for validating the QSAR  
382 models ( $r^2_{PRESS}$ ). Additionally, all QSAR models were  
383 cross-validated automatically using the leave-one-out  
384 (LOO) cross-validation (see sections QSAR Modeling  
385 under Methods and section SM-3 under Supplementary  
386 Materials). [46, 54].

387 Equation (1) shows the details of the optimal QSAR model.  
388 Figure 2 shows the corresponding scatter plots of experimen-  
389 tal versus estimated bioactivities for the training and testing  
390 inhibitors.

t1.1 **Table 1** Pharmacophoric features and corresponding weights, tolerances and 3D coordinates of Hypo34/2, Hypo37/3 and Hypo38/10. *HBA* Hydrogen  
t1.2 bond acceptors, *RingArom* aromatic rings, *Hbic* hydrophobic features

t1.2	Model	Definition	Chemical features							
t1.3			HBA		HBA		RingArom		Hbic	
t1.4	Hypo34/2 <sup>a</sup>	Weights	2.18		2.18		2.18		2.18	
t1.5		Tolerances	1.60	2.20	1.60	2.20	1.60	1.60	1.60	
t1.6		Coordinates	X	-5.14	-4.564	4.119	5.854	-0.9117	0.626	-0.8532
t1.7			Y	-3.338	-0.398	0.129	-1.018	-0.7359	-2.904	3.994
t1.8			Z	0.604	0.4555	-2.117	4.278	-1.906	-0.719	0.5818
t1.9			HBA		HBA		RingArom		Hbic	
t1.10	Hypo37/3 <sup>b</sup>	Weights	1.806		1.806		1.806		1.806	
t1.11		Tolerances	1.60	2.20	1.60	1.60	1.60	1.60	1.60	
t1.12		Coordinates	X	-0.0.51	-0.662	-0.546	-0.330	0.294	1.735	-2.706
t1.13			Y	4.744	5.735	-0.0448	-0.7208	-4.394	2.561	-1.0022
t1.14			Z	0.4635	-2.364	-0.1923	2.7225	-4.946	-6.178	-0.4202
t1.15			HBA		HBA		RingArom		Hbic	
t1.16	Hypo38/10 <sup>b</sup>	Weights	1.29		1.29		1.29	1.29	1.29	
t1.17		Tolerances	1.6	2.2	1.6	1.60	1.6	1.6	1.6	
t1.18		Coordinates	X	4.479	-0.821	-1.209	-2.949	3.058	4.221	4.573
t1.19			Y	8.359	-9.341	-14.949	-13.368	17.378	12.374	4.838
t1.20			Z	-1.982	4.907	4.779	2.915	-4.1832	-2.548	-1.419

<sup>a</sup> Hypo34/2: the 2nd pharmacophore hypothesis generated in the 34st HYPOGEN run (Table D under Supplementary Material)

<sup>b</sup> Hypo37/3: the 3th pharmacophore hypothesis generated in the 37th HYPOGEN run (Table D under Supplementary Material)

<sup>b</sup> Hypo38/10: the 10th pharmacophore hypothesis generated in the 38th HYPOGEN run (Table D under Supplementary Material)

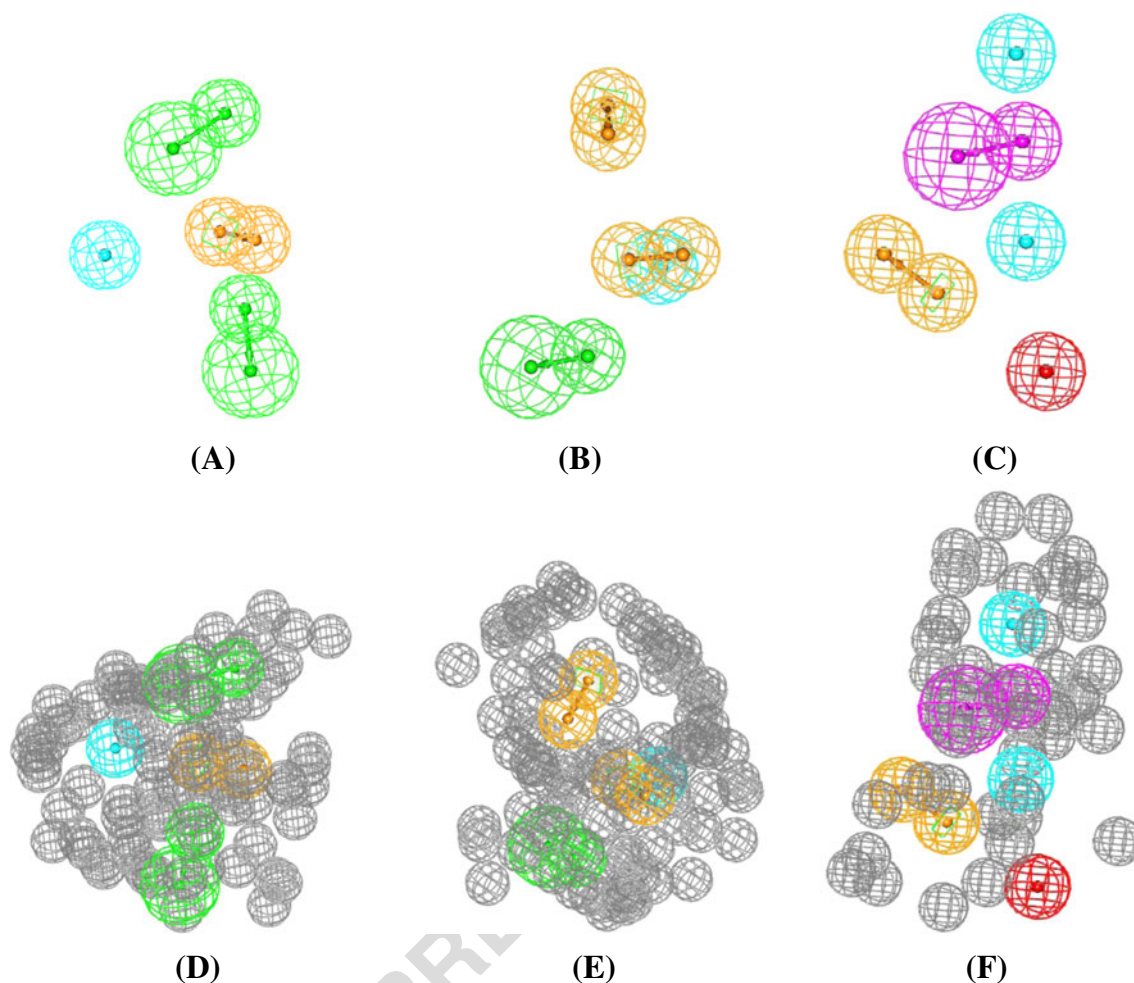


**Fig. 3** Pharmacophoric features of **a** Hypo34/2, **b** Hypo37/3 and **c** Hypo38/10. *Pink vectored spheres* Hydrogen bond doner (HBD) features, *blue spheres* hydrophobic features (Hbic), *vectored orange spheres* aromatic rings (RingArom), *green vectored spheres*

hydrogen bond acceptors (HBA), *red spheres* positive ionizable features (PosIon). **d–f** Sterically refined versions of Hypo34/2 (**d**), Hypo37/3 (**e**), and Hypo38/10 (**f**). *Gray spheres* Exclusion volumes

393  
392

$$\begin{aligned} \text{Log}\left(1/K_i\right) = & -0.41[\pm 0.13]-14.59[\pm 2.1]\text{dsN\_Count}-1.08 \times 10^{-2}[\pm 0.01]\text{dO\_Sum} \\ & +3.73[\pm 0.54]\text{dsN\_Sum}-6.08 \times 10^{-2}[\pm 0.04]\text{Num\_Rotatable Bonds} \\ & +0.13[\pm 0.024]\text{Hypo34/2} + 0.16[\pm 0.029]\text{Hypo37/3} \\ & +0.18[\pm 0.04]\text{Hypo38/10} \end{aligned}$$

394  
395  
396  
397

$$r_{\text{training}}^2 = 0.74, F_{\text{statistic}} = 64.3, r_{\text{LOO}}^2 = 0.71,$$

$$r_{\text{PRESS-test}}^2 = 0.79, \overline{r_{\text{m training}}^2} = 0.70,$$

$$\Delta r_{\text{m training}}^2 = 0.021, Q_{F1}^2 = 0.76, {}^c R_p^2 = 0.72 \dots \dots \dots$$

(1)

399 where  $r_{\text{training}}^2$  is the correlation coefficient against 162 train-  
402 ing compounds,  $F_{\text{statistic}}$  is Fisher significance criteria,  $r_{\text{LOO}}^2$  is  
403 the leave-one-out correlation coefficient, and  $r_{\text{PRESS-test}}^2$  is the  
404 predictive  $r^2$  determined for the 40 test compounds [45, 54].  
405  $\overline{r_{\text{m}}^2}$  and  $\Delta r_{\text{m}}^2$  are the average and delta  $r_{\text{m}}^2$  values. Both are

**Table 2** Receiver operating characteristic (ROC) curve analysis criteria for quantitative structure-activity relationship (QSAR)-selected pharmacophores and their sterically refined versions. *AUC* Area under the curve, *ACC* overall accuracy, *SPC* overall specificity, *TPR* overall true positive rate, *FNR* overall false negative rat

Pharmacophore model	ROC-AUC	ACC	SPC	TPR	FNR
Hypo34/2	0.75	0.97	0.98	0.77	0.02
Hypo37/3	0.83	0.97	0.98	0.92	0.02
Hypo38/10	0.99	0.97	1.00	0.13	0.003
Refined Hypo34/2	0.94	0.97	0.99	0.55	0.014
Refined Hypo37/3	0.93	0.97	0.98	0.76	0.02
Refined Hypo38/10	1.00	0.97	1.00	0.08	0.002

t2.1

t2.2

t2.3

t2.4

t2.5

t2.6

t2.7

t2.8

406 recently developed metrics that test the internal and external  
407 predictive capacities of a QSAR model extensively through

408 establishing the proximity between predicted and observed  
409 response data among 162 training compounds. QSAR models

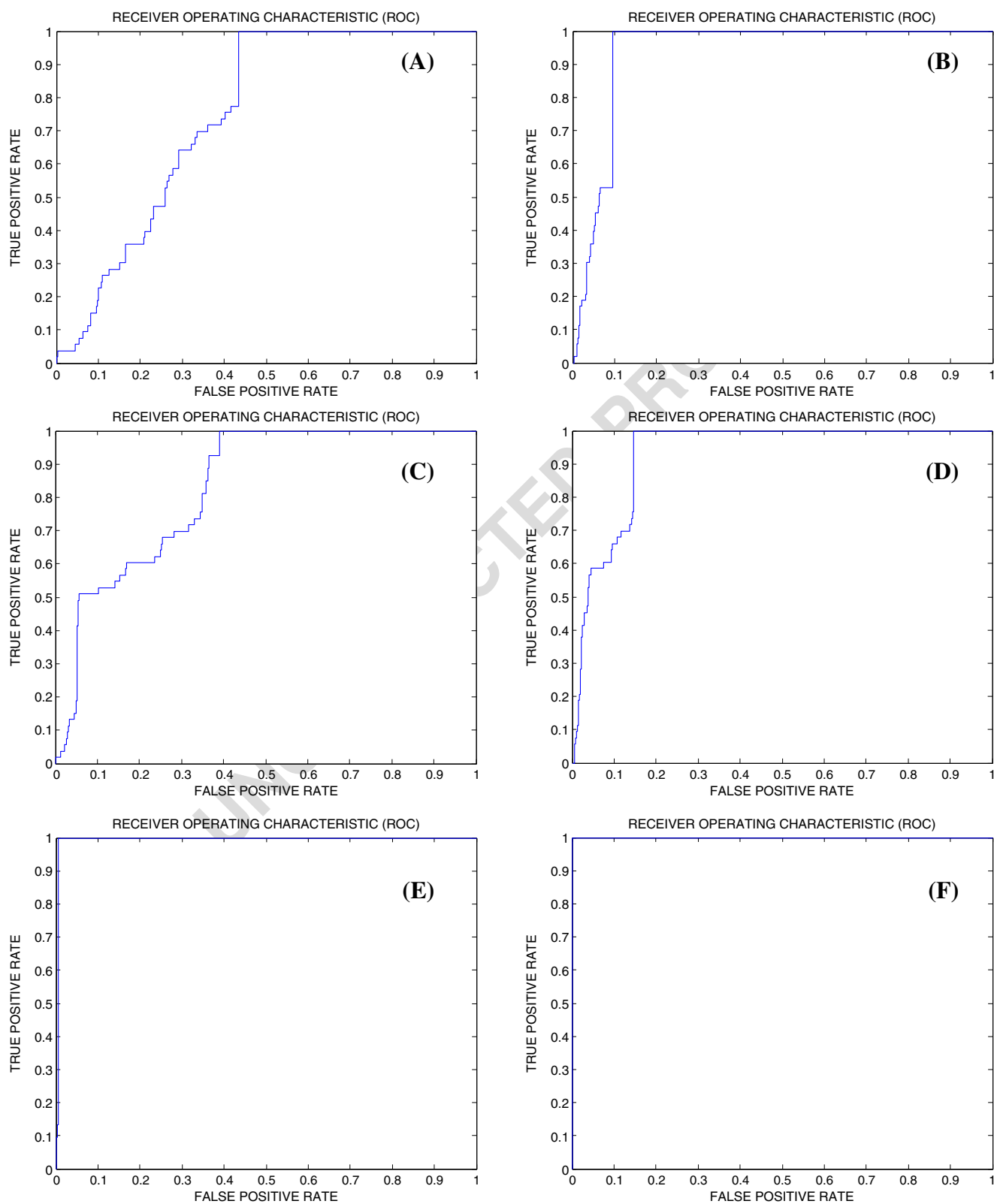


**Fig. 4** Receiver operating characteristic (ROC) curves of **a** Hypo34/2, **b** sterically refined Hypo34/2, **c** Hypo 37/3, **d** sterically refined Hypo37/3, **e** Hypo38/10, **f** sterically refined Hypo38/10



410 of  $\overline{r_m^2} > 0.5$  and  $\Delta r_m^2 < 0.2$  are considered predictive and  
 411 reliable [61, 62].  $Q_{F1}^2$  is a prediction metric proposed by Shi  
 412 et al. [63] and calculated using the external testing list (40  
 413 compounds). To further establish the statistical significance of  
 414 the QSAR model we performed Y randomization tests by  
 415 randomly shuffling the dependent variable 100 times while  
 416 keeping the independent variables as it is.  ${}^cR_p^2$  is a metric  
 417 derived from the difference between  $r_{\text{training}}^2$  and average

$r_{\text{training}}^2$  of random models.  ${}^cR_p^2$  should be  $>0.50$  for  
 418 passing this test [66]. Based on these metrics, as well as  
 419 others, QSAR Eq. (1) was found to pass Golbraikh  
 420 and Tropsha criteria [64, 65].

The reader is referred to the Supplementary Materials  
 422 (section SM-6 and Table J) to evaluate the significance  
 423 of the QSAR model through extensive list of validation  
 424 techniques.  
 425

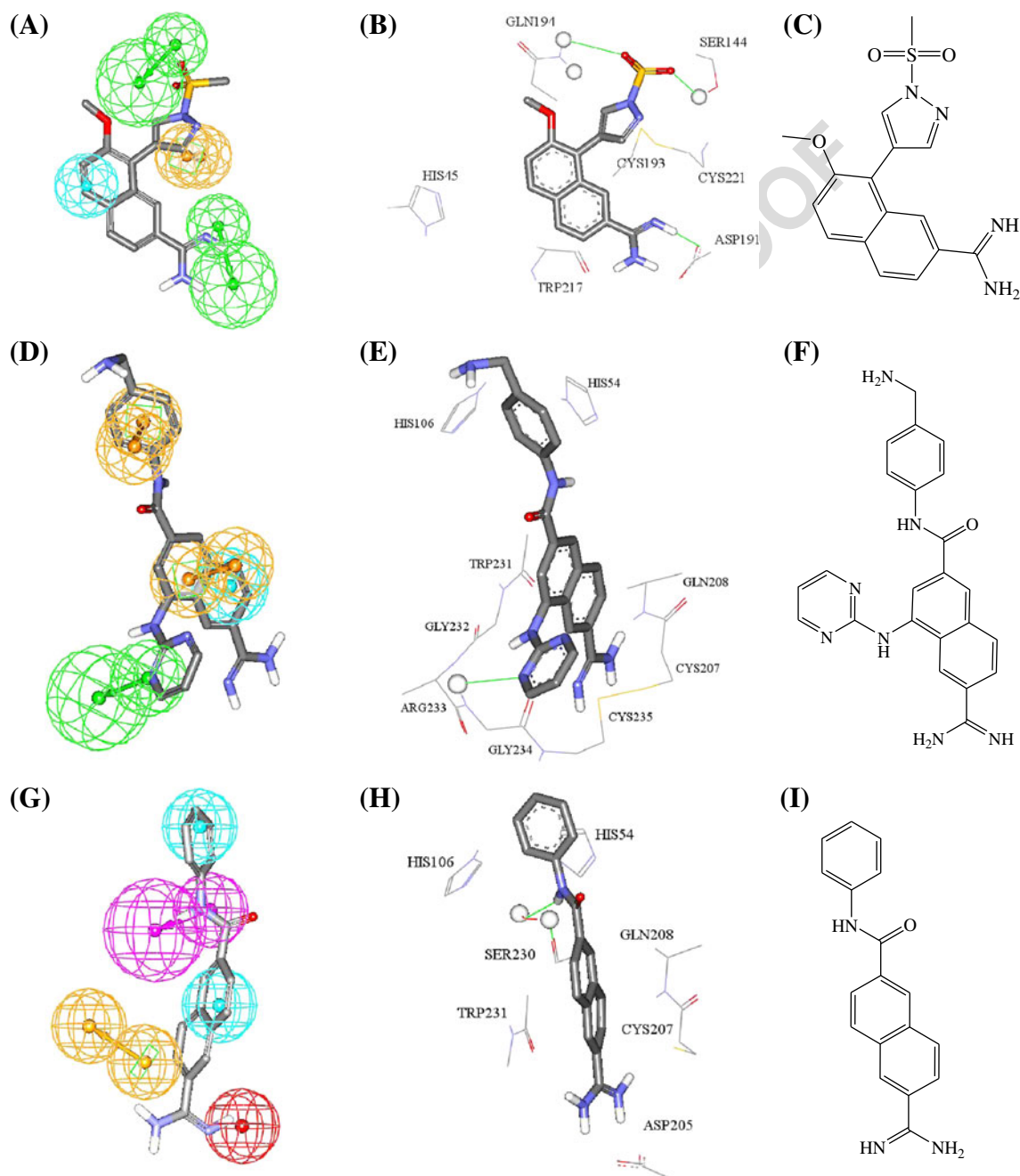


**Fig. 5** **a** Mapping of compound **148** ( $K_i=0.63 \mu\text{M}$ , Table A under Supplementary Materials) against Hypo34/2. **b** Co-crystallized complex of **148** within uPA (PDB code: 1SQT, resolution=1.90 Å). **c** Chemical structure of **148**. **d** Mapping of compound **158** ( $K_i=0.0006 \mu\text{M}$ , Table A under Supplementary Materials) against Hypo37/3. **e** Co-crystallized

complex of **158** within uPA (PDB code: 1SQA, resolution=2.0 Å). **f** Chemical structure of **158**. **g** Mapping of compound **142** against Hypo38/10. **h** Co-crystallized complex of **142** within uPA (PDB code: 1OWE, resolution=1.6 Å). **i** chemical structure of **142**

426 Hypo34/2, Hypo37/3 and Hypo38/10 (Table 1) represent  
 427 the fit values of the training compounds against these  
 428 pharmacophores (shown in Fig. 2) as calculated from equation  
 429 (D) in [Supplementary Materials](#) [33]. **dsN\_Count**,  
 430 **dsN\_Sum**, **dO\_Sum** are electrotopological state indices related  
 431 to the number of imine nitrogen (**dsN\_Count** and  
 432 **dsN\_Sum**) and ether oxygen atoms (**dO\_Sum**) in training  
 433 molecules [46]. **Num\_RotaTable Bonds** is the number of  
 434 rotatable bonds defined as any single non-ring bond, bonded  
 435 to a nonterminal heavy (i.e., non-hydrogen) atom. Amide C–  
 436 N bonds are not considered because of their high rotational  
 437 energy barrier [46]. Table H and Table I show the values  
 438 molecular descriptors of QSAR Eq. (1) as calculated for  
 439 training and testing compounds, respectively.

440 Emergence of three reasonably orthogonal pharmacophoric  
 441 models, i.e., Hypo34/2, Hypo37/3 and Hypo38/10 (Table G  
 442 under [Supplementary Material](#) shows their cross-correlation  
 443 coefficient) in Eq. (1) suggests that they represent three comple-  
 444 mentary binding modes accessible to ligands within the  
 445 binding pocket of uPA. Similar conclusions were reached  
 446 about the binding pockets of other targets based on QSAR  
 447 analysis [19–28]. Figure 3 shows Hypo34/2, Hypo37/3 and  
 448 Hypo38/10. The X, Y, and Z coordinates of the three  
 449 pharmacophores are illustrated in Table 1.

450 Interestingly, the regression slopes of the three  
 451 pharmacophore models suggest they make mediocre but rather  
 452 equivalent contributions to bioactivity. Nevertheless, these  
 453 models illustrated excellent abilities in separating active com-  
 454 pounds from inactive decoys in ROC analysis [47–49, 55].  
 455 Table 2 and Fig. 4 show the ROC results of our QSAR-  
 456 selected pharmacophores (see SM-5 Receiver Operating  
 457 Characteristic Curve Analysis under [Supplementary Materials](#)  
 458 for more details).

459 To correlate the binding features in Hypo34/2, Hypo37/3  
 460 and Hypo38/10 with ligand-receptor binding interactions an-  
 461 choring inhibitors into the binding pocket of uPA, we com-  
 462 pared the pharmacophoric features of Hypo34/2, Hypo37/3  
 463 and Hypo38/10 with the way in which they map three co-  
 464 crystallized ligands (**148**, **158** and **142**) within uPA (PDB  
 465 codes: 1SQA, 1SQT and 1OWE) [34, 57] as shown in Fig. 5.  
 466 Figure 5a,d,g compares how training compounds **148**, **158**

and **142** (Table A under [Supplementary Materials](#)) map  
 Hypo34/2, Hypo37/3 and Hypo38/10 with the way these  
 ligands bind within uPA's binding pocket (PDB code: 1SQT,  
 1SQA and 1OWE, respectively).

From Fig. 5a and b, mapping the sulfonyl oxygen of **148**  
 against a HBA in Hypo34/2 corresponds clearly to hydrogen  
 bonding interaction connecting the same sulfone group with  
 the amidic NH and OH of Gln194 and Ser144, respectively.  
 Similarly,  $\pi$ -stacking interactions anchoring the pyrazole aro-  
 matic ring of **148** against the disulfide bridge of Cys221 and  
 Cys193 seem to correspond to fitting the same pyrazole ring  
 against the aromatic ring (RingArom) feature in Hypo34/2.  
 Furthermore, fitting the terminal amidine group of **148** against  
 the hydrogen bond acceptor (HBA) feature in Hypo34/2,  
 correlates with hydrogen-bonding interactions connecting  
 the amidino group with the carboxylate residues of Asp191.  
 Finally, the fact that the naphthalene linker reside within a  
 hydrophobic pocket comprised of Cys193, Trp217 and His45  
 correspond to fitting this group against this hydrophobic fea-  
 ture (Hbic) in Hypo34/2.

Figure 5d and e compare the co-crystallized pose of **158** in  
 uPA (PDB code: 1SQA) with the way it maps Hypo37/3.  
 Mapping the heterocyclic nitrogen atom of the pyrimidinyl  
 ring against HBA features in Hypo37/3 corresponds to  
 hydrogen-bonding interaction connecting this nitrogen to the  
 peptidic NH of Gly234 (bonded to Arg233). Similarly, fitting  
 the terminal benzylamine aromatic ring of **158** against the  
 RingArom feature in Hypo37/3 agrees with  $\pi$ -stacking inter-  
 actions resulting from inserting the particular aromatic ring  
 between the imidazole rings of His54 and His106.

Similarly, mapping the naphthyl residue of **158** against  
 Hbic and RingArom features in Hypo37/3 correlates with  
 hydrophobic proximity between this substituent and hydro-  
 phobic side chains of Gly232, Cys207 and Cys235, and  $\pi$ -  
 stacking with peptidic amides of Gln208 and Trp231.

Finally, Fig. 5g and h compare the co-crystallized pose of  
**142** in uPA (PDB code: 1OWE) with the way Hypo38/10  
 maps **142**. Mapping the amide NH of **142** against HBD  
 feature in Hypo38/10 corresponds to hydrogen-bonding inter-  
 actions connecting this nitrogen to the carbonyl oxygen of  
 Ser230 via a bridging water molecule. Moreover, fitting the

t3.1 **Table 3** Numbers of captured hits by sterically refined versions of Hypo34/2, Hypo37/3 and Hypo38/10

t3.2			Pharmacophore models		
t3.3	3D Database <sup>a</sup>	Post screening filtering <sup>b</sup>	Sterically-refined Hypo34/2	Sterically-refined Hypo37/3	Sterically-refined Hypo38/10
t3.4	NCI	Before	8633	7771	145
t3.5		After	3402	5531	113

<sup>a</sup> National Cancer Institute list of available compounds (238,819 structures)

<sup>b</sup> Using Lipinski's [51] and Veber's [49] rules

t4.1 **Table 4** Predicted and experimental bioactivities of high-ranking hit molecules

Hits <sup>a</sup>	Name <sup>b</sup>	Experimental % inhibition		
		at 10 $\mu\text{M}$ <sup>c</sup>	$\text{IC}_{50}$ ( $\mu\text{M}$ ) <sup>d</sup>	
t4.4	203	135,766	63	6.3
t4.5	204	666,712	57	9.0
t4.6	205	4,367	55	11.3
t4.7	206	144,205	41	28.4
t4.8	237 <sup>e</sup>	Amiloride	42	12.3

<sup>a</sup> Chemical structures shown in Fig. 9

<sup>b</sup> NCI number

<sup>c</sup> Experimental percentage of inhibition determined at 10  $\mu\text{M}$  inhibitor concentrations

<sup>d</sup>  $\text{IC}_{50}$  values experimentally determined for most active hits

<sup>e</sup> Reported Amiloride uPA inhibitory  $\text{IC}_{50}=7.0$   $\mu\text{M}$ . [58] Each values represents the average of duplicate measurements

508 naphthalene aromatic system of **142** against RingArom and  
509 Hbic features in Hypo38/10 agrees with  $\pi$ -stacking this ring

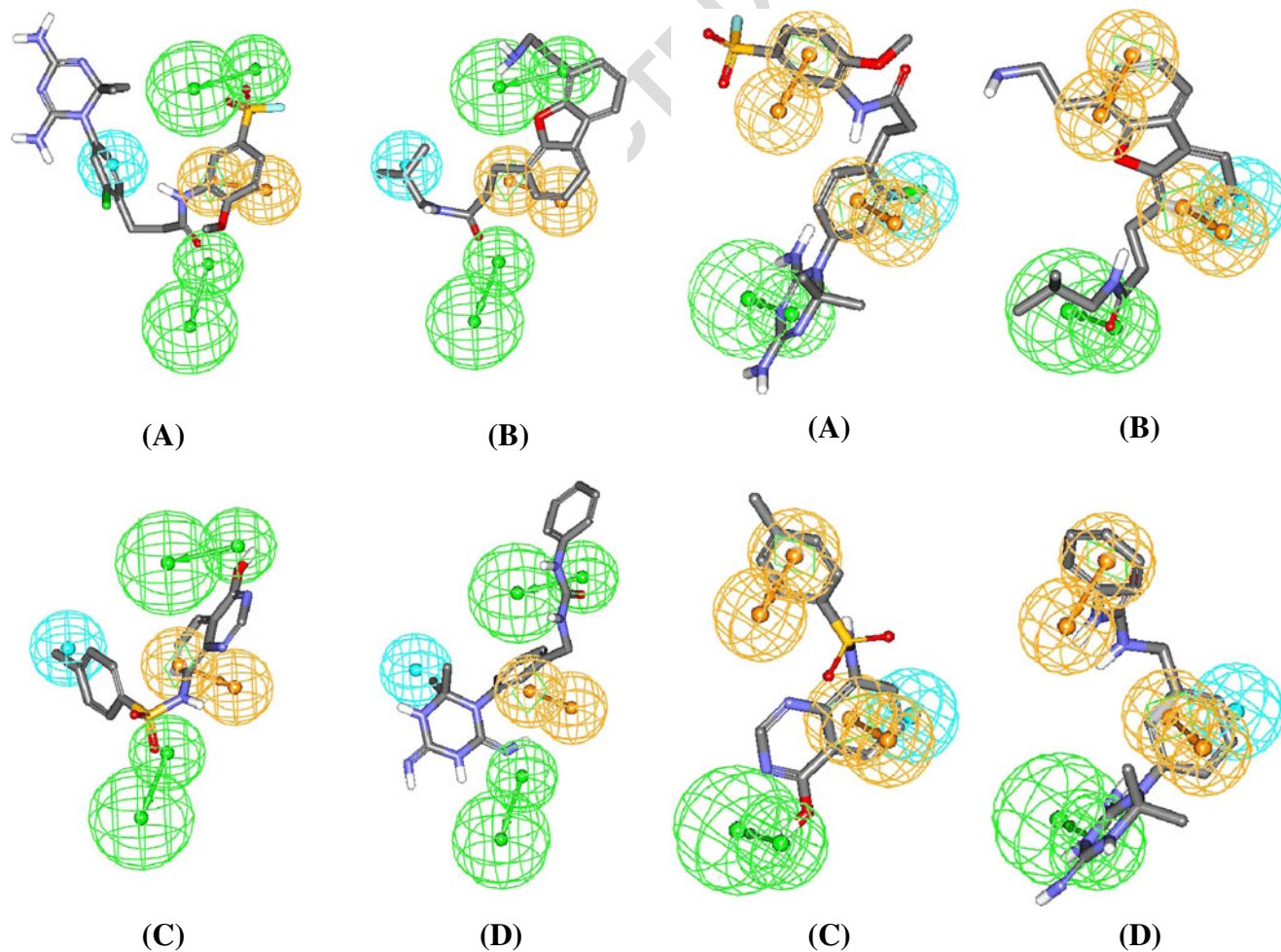


**Fig. 6** a, b, c and d show Hypo34/2 fitted against active hits **203**, **204**, **205** and **206**, respectively

system against the amidic backbone of Cys207 and Trp231 and its close proximity to the hydrophobic linker of Gln208. Additionally, mapping the terminal anilide ring of **142** against Hbic feature in Hypo38/10 agrees with stacking this ring between aromatic rings of His106 and His54. Finally, mapping the amidine of **142** against PosIon feature in Hypo38/10 corresponds to ionic attraction connecting this positive group with the carboxylate side chain of Asp205.

Steric refinement, virtual screening and in vitro validation

Pharmacophores serve as useful 3D QSAR models and 3D search queries; however, they lack the steric constraints necessary to define the size of the binding pocket. This liability renders pharmacophoric models rather promiscuous in some cases [25]. Therefore, we decided to complement the optimal pharmacophores with exclusion spheres employing the Hip-Hop-Refine module implemented within CATALYST [37]. Excluded volumes resemble sterically inaccessible regions within the binding site (see section SM-4: Hip-Hop-Refine

**Fig. 7** a, b, c and d show Hypo37/3 fitted against hits **203**, **204**, **205** and **206**, respectively



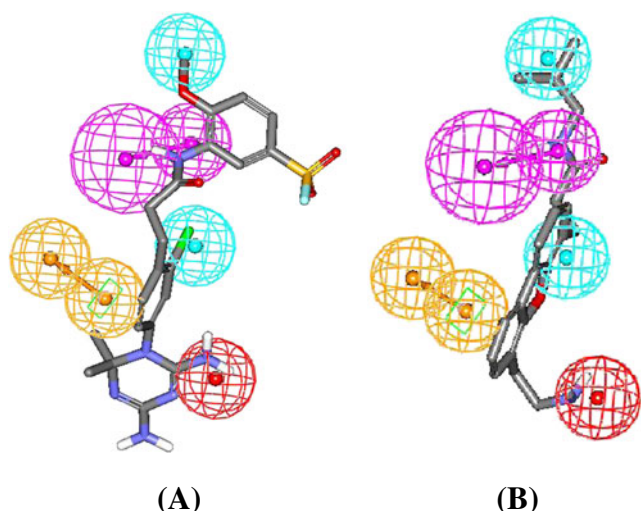
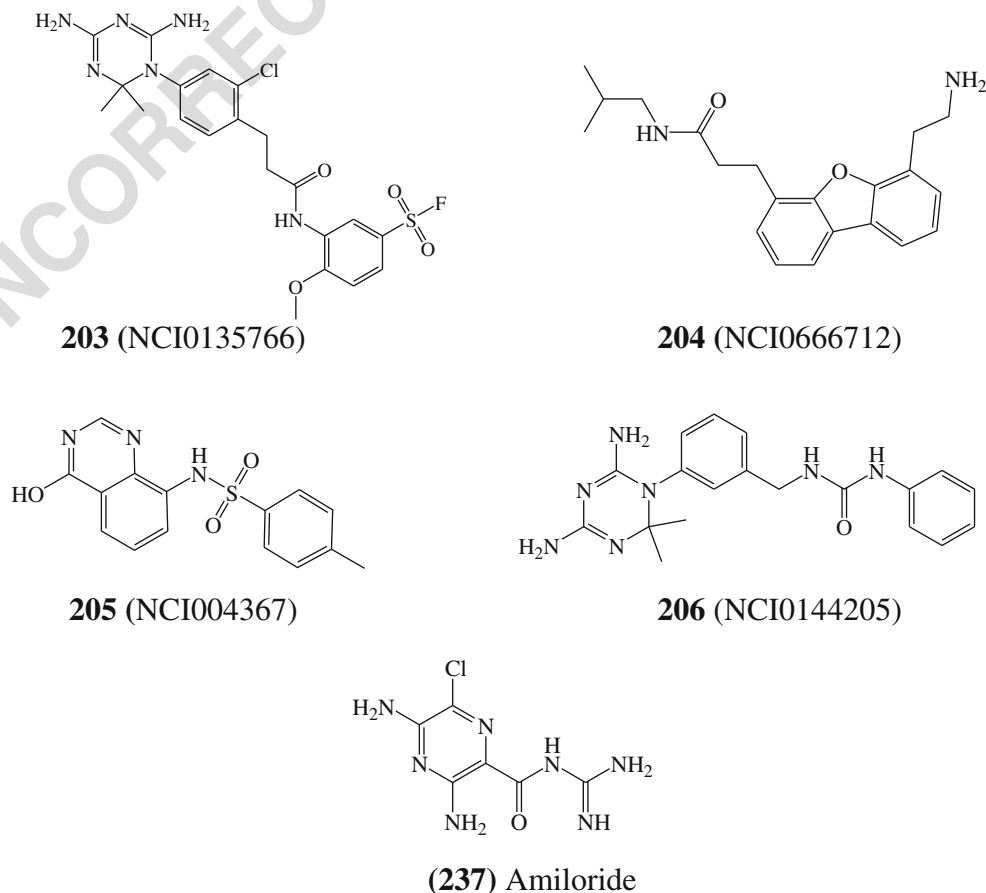


**Fig. 8** a and b show Hypo38/10 fitted against active hits **203** and **204**, respectively

528 algorithm and employed settings under [Supplementary](#)  
529 [Material](#) for more details) [56].

530 We selected a diverse training subset for Hip-Hop-Refine  
531 modeling (subset **VIII** in Table **E** under supplementary ma-  
532 terial). The training compounds were selected in such a way  
533 that the bioactivities of weakly active compounds are explain-  
534 able by steric clashes within the binding pocket.

**Fig. 9** Chemical structure of the most active hits



535 We assessed the success of steric refinement experiments  
536 through ROC analysis of the sterically refined pharmacophore  
537 versions. Table **2** shows the ROC results of the refined  
538 pharmacophores compared to their unrefined counterparts.  
539 Clearly, steric refinement improved the classification power  
540 of the three pharmacophores. This effect was particularly  
541 evident with Hypo34/2 and Hypo37/3, which had their  
542 ROC areas under the curve (AUCs) increased from  
543 75 % and 83 % to 94 % and 93 %, respectively.  
544 However, the effect of steric refinement on the efficien-  
545 cy of Hypo38/10 was less drastic. This is not surprising,  
546 since this pharmacophore is inherently of superior clas-  
547 sification power due to the presence of a PosIon fea-  
548 tures among its binding features.

549 Sterically refined Hypo34/2 (Fig. **3d**), Hypo37/3  
550 (Fig. **3e**) and Hypo38/10 (Fig. **3f**) were employed as  
551 3D search queries against the National Cancer Institute  
552 list of compounds (NCI, 238,819 structures). Table **3**  
553 summarizes the numbers of captured hits by sterically  
554 refined versions of the pharmacophores. Subsequently, cap-  
555 tured hits were filtered based on Lipinski's and Veber's rules,  
556 [50, 51]. The remaining hits were fitted against Hypo34/2,  
557 Hypo37/3 and Hypo38/10 and their fit values, together with  
558 other relevant molecular descriptors, were substituted in  
559 QSAR Eq. (1) to predict their anti-uPA bioactivities. The  
560



560 highest-ranking hits were evaluated in vitro against human  
561 uPA [52]. Figure 9 and Table 4 shows the most active hits,  
562 while Table F under supplementary material shows other less  
563 active hits. Figures 6, 7 and 8 show how the most potent hits  
564 **203**, **204**, **205** and **206** map against Hypo34/2, Hypo37/3 and  
565 Hypo38/10.

566 Interestingly, although three of our hits shared related  
567 chemical functionalities with known anti-uPA com-  
568 pounds, e.g., guanidines, amidines and sulfonamides  
569 (i.e., **203**, **205** and **206**, Fig. 9), one of the hits, i.e.,  
570 **204** ( $IC_{50}=9.0 \mu M$ , Table 4 and Fig. 9) is completely  
571 novel and represents a new class of uPA inhibitors that  
572 can be potentially optimized into interesting new drug  
573 molecules. It should be mentioned that the absence of  
574 guanidine and amidine groups from **204** should enhance  
575 the bioavailability of this class of anti-uPA agents.

## 576 Conclusions

577 uPA inhibitors are currently considered as potential  
578 treatments for cancer. The pharmacophoric space of  
579 uPA inhibitors was explored via seven diverse sets of  
580 inhibitors and using CATALYST-HYPOGEN to identify  
581 high quality binding model(s). Subsequently, genetic  
582 algorithm and multiple linear regression analysis were  
583 employed to access optimal QSAR model capable of  
584 explaining anti-uPA bioactivity variation across 202 col-  
585 lected uPA inhibitors. Three pharmacophoric models  
586 emerged in the QSAR equation suggesting the existence  
587 of more than one binding modes accessible to ligands  
588 within uPA binding pocket. The QSAR equation and the  
589 associated pharmacophoric models were validated exper-  
590 imentally by the identification of several uPA inhibitors  
591 retrieved via in silico screening, out of which three NCI  
592 hits illustrated superior potencies over the standard uPA  
593 inhibitor amiloride. Our results suggest that the combi-  
594 nation of pharmacophoric exploration and QSAR analy-  
595 ses can be useful tool for finding new diverse uPA  
596 inhibitors.

597 **Acknowledgments** The authors thank the Deanship of Scientific Re-  
598 search and Hamdi-Mango Center for Scientific Research at the University  
599 of Jordan for their generous funds. We are also thankful for NCI institu-  
600 tion for supporting us with free samples.

## 602 References

603 1. Rosenberg S (1999) The urokinase-type plasminogen activator and  
604 its receptor in cancer. *Annu Rep Med Chem* 34:121–128  
605 2. Fazioli F, Blasi F (1994) Urokinase-type plasminogen activator and  
606 its receptor: new targets for anti-metastatic therapy? *Trends*  
607 *Pharmacol Sci* 15:25–29

3. Evans DM, Sloan-Stakleff KD (1998) Maximum effect of urokinase 608  
plasminogen activator inhibitors in the control of invasion and me- 609  
tastasis of rat mammary cancer. *Invasion Metastasis* 18:252–260 610  
4. Stacey MC, Burnand KG, Mahmoud-Alexandroni M, Gaffney PJ, 611  
Bhagal BS (1993) Tissue and urokinase plasminogen activators in 612  
the environs of venous and ischaemic leg ulcers. *Br J Surg* 80:596– 613  
599 614  
5. Palolahti M, Lauharanta J, Stephens RW, Kuusela P, Vaheri A (1993) 615  
Proteolytic activity in leg ulcer exudate. *Exp Dermatol* 2:29–37 616  
6. Rogers AA, Burnett S, Moore JC, Shakespeare PG, John Chen WY 617  
(1995) Involvement of proteolytic enzymes—plasminogen activators 618  
and matrix metalloproteinases—in the pathophysiology of pressure 619  
ulcers. *Wound Repair Regen* 3:273–283 620  
7. Wysocki AB, Kusakabe AO, Chang S, Tuan T-L (1999) Temporal 621  
expression of urokinase plasminogen activator, plasminogen activa- 622  
tor inhibitor and gelatinase-B in chronic wound fluid switches from a 623  
chronic to acute wound profile with progression to healing. *Wound* 624  
*Repair Regen* 7:154–165 625  
8. Matthews H, Ranson M, Tyndall JDA, Kelso MJ (2011) Synthesis 626  
and preliminary evaluation of amiloride analogs as inhibitors of the 627  
urokinase-type plasminogen activator (uPA). *Bioorg Med Chem Lett* 628  
21:6760–6766 629  
9. West CW, Adler M, Arnaiz D, Chen D, Chu K, Gualtieri G, Ho E, 630  
Huwea C, Light D, Phillips G, Pulk R, Sukovich D, Whitlow M, 631  
Yuan S, Bryant J (2009) Identification of orally bioavailable, non- 632  
amidine inhibitors of urokinase plasminogen activator (uPA). *Bioorg* 633  
*Med Chem Lett* 19:5712–5715 634  
10. Pandya V, Jain M, Chakrabarti G, Soni H, Parmar B, Chaugule B, 635  
Patel J, Joshi J, Joshi N, Rath A, Raviya M, Shaikh M, Sairam 636  
KVVM, Patel H, Patel P (2011) Discovery of inhibitors of plasmin- 637  
ogen activator inhibitor-1: structure–activity study of 5-nitro-2- 638  
phenoxybenzoic acid derivatives. *Bioorg Med Chem Lett* 21:5701– 639  
5706 640  
11. Ye B, Bauer S, Buckman BO, Ghannam A, Griedel BD, Khim S-K, 641  
Lee W, Sacchi KL, Shaw KJ, Liang A, Wu Q, Zhao Z (2003) 642  
Synthesis and biological evaluation of menthol-based derivatives as 643  
inhibitors of plasminogen activator inhibitor-1 (PAI-1). *Bioorg Med* 644  
*Chem Lett* 13:3361–3365 645  
12. Gopalsamy A, Kincaid SL, Ellingboe JW, Groeling TM, Antrilli TM, 646  
Krishnamurthy G, Aulabaugh A, Friedrichsb GS, Crandall DL 647  
(2004) Design and synthesis of oxadiazolidinediones as inhibitors 648  
of plasminogen activator inhibitor-1. *Bioorg Med Chem Lett* 14: 649  
3477–3480 650  
13. Beeley RA, Sage NC (2003) GPCRs: an update on structural ap- 651  
proaches to drug discovery. *Targets* 2:19–25 652  
14. Klebe G (2006) Virtual ligand screening: strategies, perspectives and 653  
limitations. *Drug Discov Today* 11:580–594 654  
15. Steuber H, Zentgraf M, Gerlach C, Sottriffer CA, Heine A, Klebe GJ 655  
(2006) Expect the unexpected or caveat for drug designers: multiple 656  
structure determinations using aldose reductase crystals treated under 657  
varying soaking and co-crystallisation conditions. *Mol Biol* 363:174– 658  
187 659  
16. Stubbs MT, Reyda S, Dullweber F, Moller M, Klebe G, Dorsch D, 660  
Mederski W, Wurziger H (2002) pH-dependent binding modes ob- 661  
served in trypsin crystals: lessons for structure-based drug design. 662  
*Chem Biol Chem* 3:246–249 663  
17. DePristo MA, de Bakker PIW, Blundell TL (2004) Heterogeneity and 664  
inaccuracy in protein structures solved by X-ray crystallography. 665  
*Structure* 12:831–838 666  
18. Mertens HD, Kjaergaard M, Mysling S, Gårdsvoll H, Jørgensen TJ, 667  
Svergun DI, Ploug M (2012) A flexible multidomain structure drives 668  
the function of the urokinase-type plasminogen activator receptor 669  
(uPAR). *J Biol Chem* 287:34304–34315 670  
19. Taha MO, Bustanji Y, Al-Ghussein MAS, Mohammad M, 671  
Zalloum H, Al-Masri IM, Atallah N (2008) Pharmacophore 672  
modeling, quantitative structure–activity relationship analysis and 673






674 in silico screening reveal potent glycogen synthase kinase-3 $\beta$  inhib- 740  
 675 itory activities for cimetidine, hydroxychloroquine and gemifloxacin. 741  
 676 J Med Chem 51:2062–2077 742  
 677 20. Taha MO, Atallah N, Al-Bakri AG, Paradis-Bleau C, Zalloum H, 743  
 678 Younis K, Levesque RC (2008) Discovery of new MurF inhibitors 744  
 679 via pharmacophore modeling and QSAR analysis followed by in- 745  
 680 silico screening. Bioorg Med Chem 16:1218–1235 746  
 681 21. Taha MO, Bustanji Y, Al-Bakri AG, Yousef M, Zalloum WA, Al- 747  
 682 Masri IM, Atallah N (2007) Discovery of new potent human protein 748  
 683 tyrosine phosphatase inhibitors via pharmacophore and QSAR anal- 749  
 684 ysis followed by in silico screening. J Mol Graph Model 25:870–884 750  
 685 22. Al-masri IM, Mohammad MK, Taha MO (2008) Discovery of DPP 751  
 686 IV inhibitors by pharmacophore modeling and QSAR analysis 752  
 687 followed by in silico screening. Chem Med Chem 3:1763–1779 753  
 688 23. Taha MO, Dahabiyeh LA, Bustanji Y, Zalloum H, Saleh S (2008) 754  
 689 Combining ligand-based pharmacophore modeling, QSAR analysis 755  
 690 and in-silico screening for the discovery of new potent hormone 756  
 691 sensitive lipase inhibitors. J Med Chem 51:6478–6494 757  
 692 24. Al-Nadaf A, Abu Sheikha G, Taha MO (2010) Elaborate ligand- 758  
 693 based pharmacophore exploration and QSAR analysis guide the 759  
 694 synthesis of novel pyridinium-based potent  $\beta$ -secretase inhibitory 760  
 695 leads. Bioorg Med Chem 18:3088–3115 761  
 696 25. Abu-Hammad AM, Taha MO (2009) Pharmacophore modeling, 762  
 697 quantitative structure–activity relationship analysis, and shape- 763  
 698 complemented in silico screening allow access to novel influenza 764  
 699 neuraminidase inhibitors. J Chem Inf Model 49:978–996 765  
 700 26. Al-Sha’er MA, VanPatten S, Al-Abad Y, Taha MO (2013) Elaborate 766  
 701 ligand-based modeling reveal new migration inhibitory factor inhib- 767  
 702 itors. J Mol Graph Model 42:104–114 768  
 703 27. Al-Sha’er MA, Taha MO (2010) Discovery of novel CDK1 inhibitors 769  
 704 by combining pharmacophore modeling, QSAR analysis and in silico 770  
 705 screening followed by in vitro bioassay. Eur J Med Chem 45:4316– 771  
 706 4330 772  
 707 28. Al-Sha’er MA, Taha MO (2010) Elaborate ligand-based modeling 773  
 708 reveals new nanomolar heat shock protein 90 $\alpha$  inhibitors. J Chem Inf 774  
 709 Model 50:1706–1723 775  
 710 29. Barber CG, Dickinson RP (2002) Selective urokinase-type plasmin- 776  
 711 ogen activator (uPA) inhibitors. Part 2: (3-substituted-5-halo-2- 777  
 712 pyridinyl)guanidines. Bioorg Med Chem Lett 12:185–187 778  
 713 30. Subasinghe NL, Illig C, Hoffman J, Rudolph MJ, Wilson KJ, Soll R, 779  
 714 Randle T, Green D, Lewandowski F, Zhang M, Bone R, Spurlino J, 780  
 715 DesJarlais R, Deckman I, Molloy CJ, Manthey C, Zhou Z, Sharp C, 781  
 716 Maguire D, Crysler C, Grasberger B (2001) Structure-based design, 782  
 717 synthesis and SAR of a novel series of thiopheneamidine urokinase 783  
 718 plasminogen activator inhibitors. Bioorg Med Chem Lett 11:1379– 784  
 719 1382 785  
 720 31. Barber CG, Dickinson RP, Fish PV (2004) Selective urokinase- 786  
 721 type plasminogen activator (uPA) inhibitors. Part 3: 1- 787  
 722 Isoquinolinylguanidines. Bioorg Med Chem Lett 14:3227–3230 788  
 723 32. Barber CG, Dickinson RP, Horne VA (2002) Selective urokinase- 789  
 724 type plasminogen activator (uPA) inhibitors. Part 1: 2- 790  
 725 pyridinylguanidines. Bioorg Med Chem Lett 12:181–184 791  
 726 33. Spencer JR, McGee D, Allen D, Katz BA, Luong C, Sendzik M, 792  
 727 Squires N, Mackman RL (2002) 4-Aminoarylguanidine and 4- 793  
 728 aminobenzamidine derivatives as potent and selective urokinase- 794  
 729 type plasminogen activator inhibitors. Bioorg Med Chem Lett 12: 795  
 730 2023–2026 796  
 731 34. Wendt MD, Geyer A, McClellan WJ, Rockway TW, Weitzberg M, 797  
 732 Zhao X, Mantei R, Stewart K, Nienaber V, Klinghofer V, Giranda 798  
 733 VL (2004) Interaction with the S1b-pocket of urokinase: 8- 799  
 734 heterocycle substituted and 6,8-disubstituted 2-naphthamidine uroki- 800  
 735 nase inhibitors. Bioorg Med Chem Lett 14:3063–3068 801  
 736 35. Rudolph MJ, Illig CR, Subasinghe NL, Wilson KJ, Hoffman JB, 802  
 737 Randle T, Green D, Molloy CJ, Soll RM, Lewandowski F, Zhang M, 803  
 738 Bone R, Spurlino JC, Deckman IC, Manthey C, Sharp C, Maguire D, 804  
 739 Grasberger BL, DesJarlais RL, Zhou Z (2002) Design and synthesis 805  
 of 4,5-disubstituted-thiophene-2-amidines as potent urokinase inhib-  
 itors. Bioorg Med Chem Lett 12:491–495  
 36. StOrzebecher J, Vieweg H, Steinmetzer T, Schweinitz A, Stubbs MT, 3  
 Renatus M, WikstrOm P (1999) 3-Amidinophenylalanine-based in-  
 hibitors of urokinase. Bioorg Med Chem Lett 9:3147–3152  
 37. (2005) CATALYST 4.11 users’ manual. Accelrys Software, San 4  
 Diego 5  
 38. Sheridan RP, Kearsley SK (2002) Why do we need so many chemical 6  
 similarity search methods? Drug Discov Today 7:903–911 7  
 39. Sutter J, Güner O, Hoffmann R, Li H, Waldman M (2000) In: Güner 8  
 OF (ed) Pharmacophore perception, development, and use in drug 9  
 design. International University Line, La Jolla, pp 501–511 10  
 40. Kurogi Y, Güner OF (2001) Pharmacophore modeling and three 11  
 dimensional database searching for drug design using catalyst. Curr 12  
 Med Chem 8:1035–1055 13  
 41. Poptodorov K, Luu T, Langer T, Hoffmann R (2006) In: Hoffmann 14  
 RD (ed) Methods and principles in medicinal chemistry. 15  
 Pharmacophores and pharmacophores searches, vol 2. Wiley-VCH, 16  
 Weinheim, pp 17–47 17  
 42. Li H, Sutter J, Hoffmann R (2000) In: Güner OF (ed) Pharmacophore 18  
 perception, development, and use in drug design. International 19  
 University Line, La Jolla, pp 173–189 20  
 43. Bersuker IB, Bahçeci S, Boggs JE (2000) In: Güner OF (ed) 21  
 Pharmacophore perception, development, and use in drug design. 22  
 International University Line, La Jolla, pp 457–473 23  
 44. (2005) CERIU2 LigandFit user manual (version 4.10). Accelrys, 24  
 San Diego, pp 3–48 25  
 45. Fischer R (1966) The principle of experimentation illustrated by a 26  
 psychophysical experiment. Hafner, New York, Chapter II 27  
 46. (2005) CERIU2, QSAR users’ manual, version 4.10 Accelrys, San 28  
 Diego, 43–88, 221–235, 237–250 29  
 47. Kirchmair J, Markt P, Distinto S, Wolber G, Langer T (2008) 30  
 Evaluation of the performance of 3D virtual screening protocols: 31  
 RMSD comparisons, enrichment assessments, and decoy selec- 32  
 tion—what can we learn from earlier mistakes? J Comput Aided 33  
 Mol 22:213–228 34  
 48. Irwin JJ, Shoichet BK (2005) ZINC—a free database of commercial- 35  
 ly available compounds for virtual screening. J Chem Inf Comput Sci 36  
 45:177–182 37  
 49. Triballeau N, Acher F, Brabet I, Pin J-P, Bertrand H-O (2005) Virtual 38  
 screening workflow development guided by the “receiver operating 39  
 characteristic” curve approach. Application to high-throughput 40  
 docking on metabotropic glutamate receptor subtype 4. J Med 41  
 Chem 48:2534–2547 42  
 50. Veber DF, Johnson SR, Cheng HY, Smith BR, Ward KW, Kopple KD 43  
 (2002) Molecular properties that influence the oral bioavailability of 44  
 drug candidates. J Med Chem 45:2615–2623 45  
 51. Lipinski CA, Lombardo F, Dominy BW, Feeney PJ (2001) 46  
 Experimental and computational approaches to estimate solubility 47  
 and permeability in drug discovery and development settings. Adv 48  
 Drug Del Rev 46:3–26 49  
 52. uPA Activity Assay kit Cat.No. ECM600. [http://www.millipore.com/  
 catalogue/item/ecm600](http://www.millipore.com/catalogue/item/ecm600) 50  
 53. Van Drie JH (2003) Pharmacophore discovery—lessons learned. 51  
 Curr Pharm 9:1649–1664 52  
 54. Ramsey LF, Schafer WD (1997) The statistical sleuth, 1st edn. 53  
 Wadsworth, Belmont 54  
 55. Verdonk ML, Marcel L, Berdini V, Hartshorn MJ, Mooij WTM, 55  
 Murray CW, Taylor RD, Watson P (2004) Virtual screening using 56  
 protein-ligand docking: avoiding artificial enrichment. J Chem Inf 57  
 Comput Sci 44:793–806 58  
 56. Clement OO, Mehl AT (2000) Pharmacophore perception, develop- 59  
 ment, and use in drug design. In: Güner OF (ed) IUL biotechnology 60  
 series. International University Line, La Jolla, pp 71–84 61  
 57. Wendt MD, Rockway TW, Geyer A, McClellan W, Weitzberg M, 62  
 Zhao X, Mantei R, Nienaber VL, Stewart K, Klinghofer V, Giranda 63

- 806 VL (2004) Identification of novel binding interactions in the devel- 823  
807 opment of potent, selective 2-naphthamidine inhibitors of urokinase. 824  
808 Synthesis, structural analysis, and SAR of N-phenyl amide 6- 825  
809 substitution. *J Med Chem* 47:303–324
- 810 58. Vassalli J-D, Belin D (1987) Amiloride selectively inhibits the 826  
811 urokinase-type plasminogen activator. *FEBS Lett* 214:187–191 827
- Q2 812 59. Roy K, Chakraborty P, Mitra I, Ojha PK, Kar S, Narayan R (2013) 828  
813 Some case studies on application of “rm2” metrics for judging quality 829  
814 of QSAR predictions: emphasis on scaling of response data. *J* 830  
815 *Comput Chem* 34:1071–1082 831
- Q3 816 60. Roy K, Mitra I (2011) On various metrics used for validation of 832  
817 predictive QSAR models with applications in virtual screening and 833  
818 focused library design. *Comb Chem High Throughput Screen* 14: 834  
819 450–474 835
- 820 61. Roy K, Mitra I, Kar S, Ojha PK, Das RN, Kabir H (2012) 836  
821 Comparative studies on some metrics for external validation of 837  
822 QSPR models. *J Chem Inf Model* 52:396–408 838Q4  
840 62. Ojha PK, Mitra I, Das RN, Roy K (2011) Further exploring rm2 839Q5  
metrics for validation of QSPR models dataset. *Chemom Intell Lab*  
*Syst* 107:194–205  
63. Shi LM, Fang H, Tomg W, Wu J, Perkins R, Blair RM, 826  
Branham WS, Dial SL, Moland CL, Sheenan DM (2001) 827  
QSAR models using a large diverse set of estrogens. *J* 828  
*Chem Inf Comput Sci* 41:186–195 829  
64. Golbraikh A, Tropsha A (2002) Beware of q2. *J Mol Graph Model* 830  
20(4):269–276 831  
65. Tropsha A (2010) Best practices for QSAR model development, 832  
validation, and exploitation. *Mol Inf* 29:476–488 833  
66. Mita I, Saha A, Roy K (2010) Exploring quantitative structure– 834  
activity relationship studies of antioxidant phenolic compounds ob- 835  
tained from traditional Chinese medicinal plants. *Mol Simulat* 36: 836  
1067–1079 837  
67. <http://aptsoftware.co.in/DTCMLRWeb> 838Q4  
68. <http://www.aptsoftware.co.in/rmsquare> 839Q5

UNCORRECTED PROOF

## AUTHOR QUERIES

### AUTHOR PLEASE ANSWER ALL QUERIES.

-  Q1. Ref. 53 was not cited anywhere in the text. Please provide a citation. Alternatively, delete the item from the list.
-  Q2. Ref. 59 was not cited anywhere in the text. Please provide a citation. Alternatively, delete the item from the list.
-  Q3. Ref. 60 was not cited anywhere in the text. Please provide a citation. Alternatively, delete the item from the list.
-  Q4. Ref. 67 was not cited anywhere in the text. Please provide a citation. Alternatively, delete the item from the list.
-  Q5. Ref. 68 was not cited anywhere in the text. Please provide a citation. Alternatively, delete the item from the list.

UNCORRECTED PROOF